Preprint
UCRL-JC-134864

Glass, Plastic & Semiconductors: Packaging Techniques for Miniature Optoelectronic Components

M.D. Pocha, H.E. Garrett, R.R. Patel, L.M. Jones II, M.C. Larson, M.A. Emanuel, S.W. Bond, R.J. Deri, R.F. Drayton, H.E. Petersen, M.E. Lowry

This article was submitted to
BIOS 2000 International Symposium on Biomedical Optics, San Jose, CA, January 22-28, 2000

December 20, 1999

U.S. Department of Energy
Lawrence Livermore National Laboratory

Glass, Plastic & Semiconductors: Packaging Techniques for Miniature Optoelectronic Components

Michael D. Pocha, Henry E. Garrett, Rajesh R. Patel, Leslie M. Jones II, Michael C. Larson, Mark A. Emanuel, Steven W. Bond, Robert J. Deri[a], Rhonda F. Drayton[b], Holly E. Petersen, Mark E. Lowry

Lawrence Livermore National Laboratory PO Box 808, L-222, Livermore, CA 94551
[a]Terawave Communications Inc., Hayward, CA
[b]University of Minnesota, Department of Electrical and Computer Engineering, Minneapolis, MN

ABSTRACT

At Lawrence Livermore National Laboratory, we have extensive experience with the design and development of miniature photonic systems which require novel packaging schemes. Over the years we have developed silicon micro-optical benches to serve as a stable platform for precision mounting of optical and electronic components. We have developed glass ball lenses that can be fabricated in-situ on the microbench substrate. We have modified commercially available molded plastic fiber ribbon connectors (MT) and added thin film multilayer semiconductor coatings to create potentially low-cost wavelength combiners and wavelength selective filters. We have fabricated both vertical-cavity and in-plane semiconductor lasers and amplifiers, and have packaged these and other components into several miniature photonics systems.

For example, we have combined the silicon optical bench with standard electronic packaging techniques and our custom-made wavelength-selective filters to develop a four-wavelength wavelength-division-multiplexing transmitter module mounted in a standard 120-pin ceramic PGA package that couples light from several vertical-cavity-surface-emitting-laser arrays into one multimode fiber-ribbon array. The coupling loss can be as low as 2dB, and the transmitters can be operated at over 1.25 GHz. While these systems were not designed for biomedical or environmental applications, the concepts and techniques are general and widely applicable.

Keywords: silicon microbench, packaging, multiwavelength VCSELS, ball lenses, wavelength selective filters, WDM, optical communications

1. INTRODUCTION

In biomedical and environmental applications, as in other systems, there is a trend toward increasing use of miniature optoelectronic components and subsystems. The addition of optical signals to electronic systems has several advantages. An example is greater bandwidth achievable in a very small space. Optical fibers are typically much smaller than coaxial cable for instance. Another important factor in biomedical systems is electrical isolation that can be achieved with optical signaling. But, the addition of optical signals also adds complexity. Now, both electrical and optical connections must be made to devices and packages. The optical connections are often done by use of optical fiber. One of the main issues becomes the alignment tolerances which must be achieved in order to make connections using optical fiber. While electrical connections require 10s to 100s of micrometer alignment precision in typical silicon integrated circuits, optical connections typically require sub-micrometer to a few micrometer tolerances. Also, unlike electrical connections, waveguiding or focusing is required for even very small distances to prevent large signal losses. A flexible, low-cost optoelectronic packaging scheme requires the development of several new techniques for managing these constraints.

At Lawrence Livermore National Laboratory we have chosen a set of packaging techniques for multimode fiber optic interconnection systems which provides a low cost solution for the required tolerances and waveguide continuity using a variety of common materials. The basis for the packaging is silicon substrates mounted in conventional electronic packages. We use ceramic and metal packages for convenience, but these techniques could also be applied to plastic packages. Silicon is a strong, hard and stiff material which provides a stable micro-optical base or micro-bench to support the optical components as well as electronic components and to maintain positional tolerances. We have developed a technique for in-situ fabrication of miniature glass ball lenses for focusing. We are developing our own optical sources including both in-plane and vertical cavity semiconductor lasers. Finally, we are modifying commercial molded plastic fiber ribbon connectors

to provide the continuously waveguided links between components. Our application is a wide bandwidth multimode fiber wavelength division multiplexed interconnect link which may not be directly applicable to biomedical or environmental applications, but serves to demonstrate the more general technology.

2. SILICON MICROBENCHES

The fundamental reason for the high cost of optoelectronic packaging can be traced to the sub-micron positional tolerances that are usually required for the packaging (or fiber optic pigtailing) of high-performance optoelectronic components. For example measurements of the coupling efficiency of single mode fiber to edge emitting lasers indicate that tolerances as low as ± 0.2 μm are needed if the fiber are lensed to maximize coupling. The tolerance can be looser if the fiber is not lensed, but a significant loss in coupling efficiency is the trade-off. Manually achieving such precision is extremely labor intensive and expensive. We will briefly discuss below two approaches that we are pursuing that can help to minimize these costs. The first is an automated fiber alignment and attachment system, and the second is the silicon microbench. The microbench concept can also be applied to the coupling of multimode lasers and fibers where the tolerances can be loosened to > ± 5.0 μm.

2.1 Automated optoelectronic packaging

Automation of the precision positioning may help reduce the costs of optoelectronic (o/e) components. In an attempt to quantitatively analyze what might be a tolerable cost of such an automated positioning machine and what an economically sensible market volume might be, we have developed a simple model that relates the cost per pigtail to the volume of components that are packaged.

$$C = (C_{op}\,(r/R) + C_{eq})/r + C_{mat}$$

where C_{eq} is the cost per unit time of the machine (we assume that it has a 5 year lifetime), C_{mat} is the material costs for each packaged device, C_{op} is the cost per unit time of the person operating the machine, r is the market demanded production rate, and R = machine limited rate of production. These equations are plotted in figure 1 for various values of the parameters. Note that as the speed of the machine goes up (time per pigtail decreases) high volume packaging becomes very inexpensive, as one might expect.

It is further interesting to note that as the machine cost goes down, money is saved by automating at lower volumes. Thus a low-cost machine will provide the economic drive for automation at surprisingly small market volumes.

As can be seen in figure 1, o/e packaging using this automated machine is expected to be cheaper than manual packaging at pigtail volumes just over 100 per year. This volume would appear to be well within the present market reach of most o/e manufacturers including small companies.

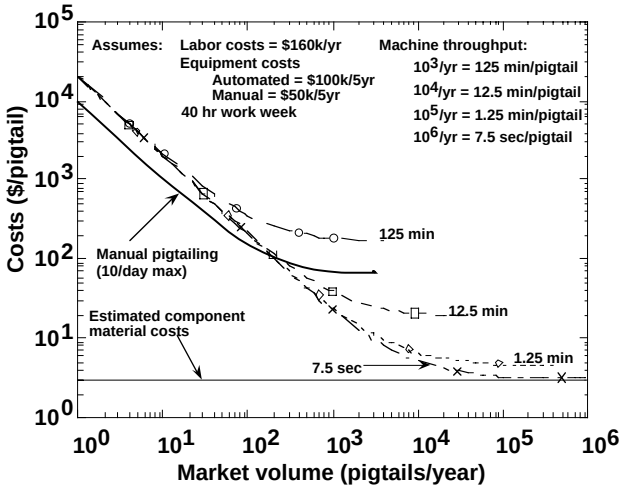

Figure 1 Results of packaging cost model.

Our approach to automation, an Automated Fiber Pigtailing Machine (AFPM) [1], is outside the scope of this discussion. In the following discussion, we concentrate on a silicon microbench technology that is compatible with automated parts placement and pigtailing.

2.2 Silicon microbenches with manufacturable solder reflow

There is a large body of literature on the exploitation of the etching properties of Si to produce v-grooves mesas, and positional stops on silicon substrates to "passively" align optical components. Much work has also been done exploring the use of "solder bumps" to precisely position components in a passive sense. In the interests of space, we make no attempt to

review that large body of work, rather we briefly describe what we believe to be an interesting adjunct to these two important packaging technologies.

Over ten years ago, miniature metallic heaters to reflow solder for the attachment of o/e components on ceramic waferboards were developed[2]. Since then many variations of this concept have been tried. We have developed silicon microbenches with integrated polysilicon heaters to improve the manufacturability of soldered silicon o/e packages[3].

Our initial work involved the development of silicon microbenches to pigtail high-powered 800 nm laser diodes to single-mode fibers. The success of the prototype has led us to develop several new designs. For example, the microbench shown in figure 2 is for packaging a 1550 nm DFB laser.

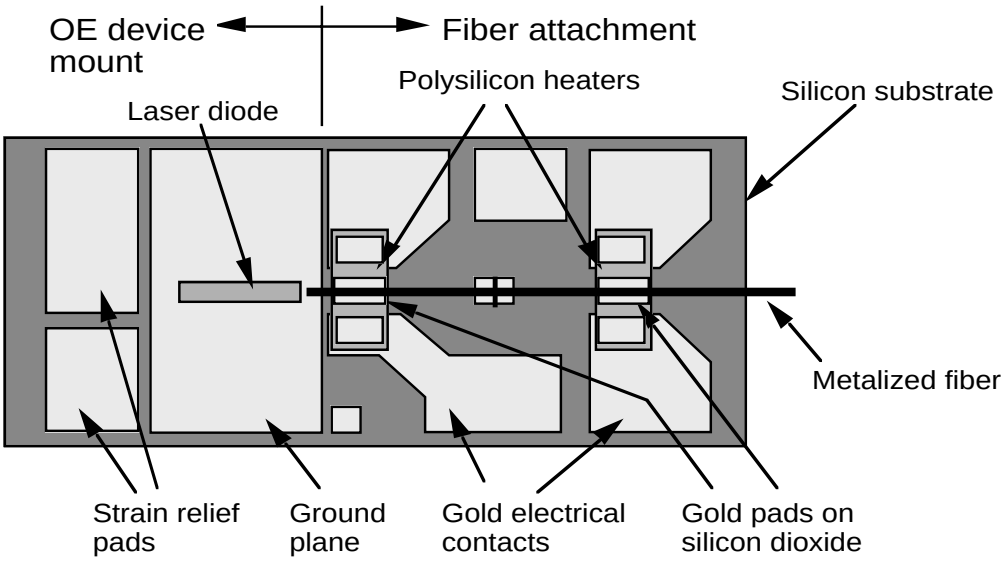

Figure 2 Silicon microbench with built-in polysilicon heaters for manufacturable solder reflow.

On the left side of the microbench, we photolithographically pattern gold pads to provide a ground plane for the laser and strain relief for the wire bonds. To attach the fiber on the other side of the microbench, we build two heating elements of polysilicon which are attached to gold bonding pads for electrical contact. In the center of each heater, we pattern a gold pad on a layer of silicon dioxide. This gold pad provides the solder attachment base while the silicon dioxide electrically isolates the gold pad from the polysilicon heater. The gold pads are 1 mm by 0.5 mm each and are sufficiently large to solder up to a 250 micron diameter fiber at the two attachment pads. We have used either 100-micron diameter solder balls or solder paste to attach the metallized fiber.

Construction of our silicon microbenches begins with a single-crystal silicon wafer as a substrate. We use a standard silicon wafer thickness of 400-500μm. Wells and pedestals are etched into the silicon as needed to approximately align, in the vertical direction, the optical axis of the various components to be mounted. Next a thick layer of silicon dioxide (SiO_2) is deposited and etched to provide some degree of thermal isolation of other areas from the heaters. The thermal resistance of SiO_2 is approximately two orders of magnitude greater than that of silicon so a 5μm thick layer of SiO_2 is thermally equivalent to a 500μm thick layer of silicon. With plasma-assisted Chemical Vapor Deposition, it is possible to deposit layers of SiO_2 up to 20-30μm thick. We generally use a thickness of 5-10μm depending on the needs of each application.

The heaters are made by depositing, doping, and patterning an approximately 1μm thick layer of polycrystalline silicon (polysilicon). The doping is adjusted to result in a resistance of the heaters of approximately 10-50Ω. Resistors in this range give the greatest control at the temperatures of interest with standard laboratory power supplies. A thin silicon dioxide layer on top of the polysilicon provides electrical isolation of the solder attachment pads to prevent shorting out of heaters. This step is not always necessary. Because of the excellent thermal conduction of silicon, it is often acceptable to allow current to flow through the solder attachment pads as long as there is an adjacent region of non-metallized polysilicon that can act as a heater.

A final metal layer of a standard Cr/Au or Ti/Au metallization completes the interconnect structure to provide electrical connections to the heaters and a layer of metal that is strongly adherent to both silicon and SiO_2 and to which most standard solders will adhere.

The performance of the polysilicon heaters on our prototype is very reproducible with a specially constructed power supply that allows us to accurately control the magnitude and time of the applied current. For single mode applications fiber positioning is done by active alignment to sub-micrometer tolerances. We typically apply one amp of current for approximately 0.5 sec to reflow solder at the fiber attachment points. We observe up to 65% optical coupling with conically machined and lensed fiber end-facets.

Our microbench geometry with on-board heaters also allows rapid attachment of the other components to be placed on the microbench. Applying larger currents for longer periods of time allows solder reflow at some distance from the heaters. Using solders with different melting temperatures and judiciously choosing the order of attachment allows a variety of components to be soldered to the microbench without movement of previously attached components.

Generally, components furthest from a heater are attached first using a high current through the heater. We can manually place and solder a thermoelectric cooler, a thermistor, and a laser diode onto our microbench at different distances from the heaters in less than 15 minutes. We envision that the placement and soldering of these components, which does not require sub-micron alignment, could be performed by an automated system in less than a minute. As the last step, the fiber must be aligned to sub-micron tolerances and is attached using the least current through the heaters. For multi-mode applications, mechanical stops can be etched on the microbench to allow for passive alignment of components which greatly simplifies and speeds up both manual and automated packaging.

These microbenches are fabricated using standard silicon microelectronics processing technology. Several hundred parts can be fabricated simultaneously on a single silicon wafer. For simple designs that do not require a well or pedestal etched in the wafer, or insulated attachment pads, we can fabricate a batch of microbenches using a single photolithographic mask. In that case the cost per part can be much less than $0.50.

We also use a standard silicon etching technique employing a potassium hydroxide (KOH) solution to etch wells (& pedestals) in the silicon substrate that can be as deep as 200 μm with a tolerance of less than ± 5 μm. This etch technique is compatible with v-groove formation used by others to precisely place fibers on microbenches, and allow precise vertical alignment of the optical axes of components mounted on the microbench. Newer reactive ion plasma etching techniques are also used for near vertical wall etching of silicon to form mechanical stops and pedestals.

The idea of on-board heaters lends itself to applications other than packaging laser diodes. We are also investigating geometries compatible with high speed applications in which on-board transmission lines will be needed to provide sufficient bandwidth for the o/e device.

3. MINIATURE GLASS BALL LENSES

An extension of silicon optical microbench fabrication is the fabrication of miniature glass ball lenses in-situ on silicon substrates. First, a series of pedestals are fabricated on a silicon substrate, by etching for example. One can then use well known glass to silicon bonding techniques to attach a sheet of glass of the appropriate thickness, pattern the glass to form rectangular or cubic prisms which, when reflowed in a high temperature furnace will form into almost perfectly spherical balls centered on the pedestals. The formation of the spheres is due to surface tension forces which also tend to provide a very smooth finish to the surfaces of the spheres allowing them to be used as lenses. Figure 3 is an example of one such lens. We have fabricated a variety of such lenses ranging in diameter from about 200 μm to almost 1 mm.

The lens in Fig. 3 was fabricated by using a precision dicing saw to cut both the pedestals in the silicon substrate (by making 90 degree cross cuts) and to form the original rectangular prisms of glass. Subsequent to cutting the glass was reflowed at a temperature of 850 °C. We note that the diameter of the ball determines it's focal length. So to accurately achieve a given focal length, the diameter must be accurately controlled.

An indirect measure of the sphericality or figure of a lens is to measure the coupling efficiency of light through the lens. Such a measurement was made with several of the lenses we fabricated. We used approximately 5 μm core diameter single mode optical fiber to make the measurement. First two cleaved fibers were brought as close as possible without actually touching (< 5 μm gap) and the peak optical power coupling was measured. Then the fibers were pulled apart and a ball lens inserted in between to form a 1:1 image of the input fiber on the output fiber. Fiber position was iteratively optimized for maximum coupling and a second light power measurement was made. The results were that over 90% of the light is coupled from the input fiber to the output fiber. Reflection losses at the two glass-air interfaces account for 8% of the 10% loss. Therefore, we can conclude that less than 2% of the light is lost due to defects or non-sphericality of the lenses.

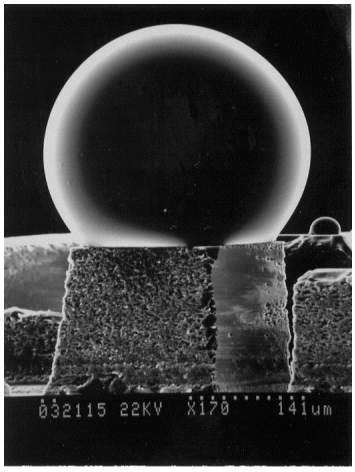

Figure 3 Glass micro ball lens fabricated on a pedestal formed in a silicon substrate by use of a dicing saw.

Since the ball is almost spherical, the diameter of the final shape is determined by the total volume of glass in the rectangular prism that is formed before reflow. It is difficult to get an exact shape in glass by etching because there is not an equivalent of crystal plane defined etching or deep vertical wall reactive ion etching that is available in silicon. Several tool manufacturers are working on such an etching process for glass, but none is available currently. We have, therefore, chosen precision sawing as a technique for patterning the glass. Since precision sawing is a linear patterning technique, it requires that the lenses be in straight lines if there are multiples of them on a given microbench. Luckily, since light also travels in straight lines this is not a very severe constraint. The accuracy of the sawing is an issue, but here we are helped by the geometry of the lenses. Since the diameter is determined by the volume of the lens, variations are a function of the cube root of any linear error. Today's state-of-the-art precision dicing saws can achieve cut dimensions with tolerances of 1-3 μm. This means that ball diameters and therefore focal length accuracy of less than 1% is possible.

The requirement for high temperature reflow is somewhat of a severe constraint because it prevents us from patterning metal interconnects on the silicon wafers before performing the glass reflow. After reflow the lenses sticking up above the silicon surface make it difficult to spin resist and print patterns of any kind. A potential solution to this problem is to build the microbench out of two silicon wafers sandwiched together. One would have the ball lenses on it and the other the metal patterns, etc. for mounting optical components with holes etched in this wafer for the ball lenses from the first substrate to stick up through. Again we can align two such wafers and bond them together with accuracies of a few μm.

4. FILTERS AND WAVEGUIDES

Parallel optical interconnects based on multimode fiber (MMF) ribbon cable are emerging as a robust, high-performance data link technology which increases channel bandwidth by using linear MMF arrays. While this technology has primarily been implemented as single wavelength point-to-point links, it can be significantly enhanced by wavelength division multiplexing (WDM). WDM enables both increased point-to-point bandwidth as well as more complex interconnect topologies and routing approaches that are particularly attractive for high performance computing platforms[4]. Exploiting the potential richness of WDM interconnects, however, also requires a low-loss routing fabric that includes small footprint wavelength selective filters. Low insertion loss is critical for this technology because the transceivers exhibit link power budgets well below that of telecom WDM systems and because the MMF cabling precludes the use of optical amplifiers. While high performance filters can be realized for single-fiber applications, achieving high-performance, small footprint devices with ribbon cable is significantly complicated by MMF's high numerical aperture (NA=0.275) and large core diameter (62.5μm).

We have developed both 2-port and 3-port filter modules assembled in simple, robust packages. Our 3-port modules are suitable for add/drop multiplexing while the 2-port devices are suitable for broadcast and select architectures. Here, we present a summary of our work on both 3-port and 2-port filter modules.

4.1 Filter Packaging Issues

Figure 4 shows the geometry of our filter modules while figure 5 provides a perspective view of a 2-port module to aid in

visualization. A high refractive index (>3.0) interference filter is sandwiched between parallel arrays of 12 MMFs using an assembly of modified commercial 'MT' fiber ribbon connector ferrules[5]. The high filter index enables narrow passbands and sharp filter edges for the high MMF numerical aperture, without additional micro-optic collimation. Furthermore, for the 3-port modules, the use of high-index materials facilitates a large angle of incidence to ease opto-mechanical packaging while minimizing bandpass spreading and polarization sensitivity. The use of commercial ferrules minimizes device size (2.7 X 6.4 X 7.6 mm^3 for 2-port modules and 5.7 X 6.4 X 7.8 mm^3 for 3-port modules), and simplifies assembly and packaging via passive alignment using guide pins. For the 2-port modules, alignment is 100% passive with the guide pins, while for the 3-port modules, the longitudinal alignment of port 3 along the port 1-2 axis is done by active alignment – this could be eliminated in production by a modified ferrule design. In addition, these modules mate directly with MT-terminated fiber ribbon cables without the need for additional connectors. The minimal complexity of the assembly, coupled with the plastic molding used to realize the ferrules, indicates the potential for cost-effective manufacture of such devices.

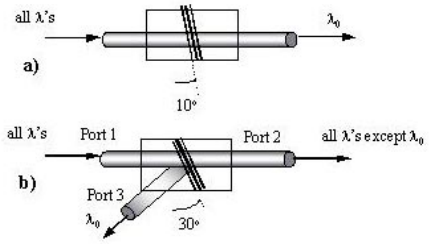

Figure 4 Schematic of a) 2-port and b) 3-port filter modules

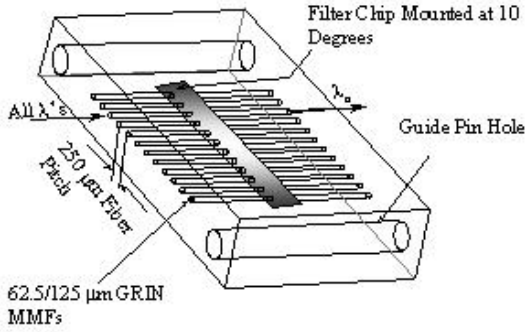

Figure 5 Perspective view of 2-port filter module packaged to be compatible with MT ferrules

4.2 Filter Design

Our 3-port devices employ a simple Bragg reflector consisting of 31 Bragg pairs as the wavelength selective element. In the 2-port configuration we have demonstrated both single cavity Fabry-Perot type filters and more complex multiple-cavity Fabry-Perot (MC-FP) filters. The filters use epitaxially grown $Al_{0.15}Ga_{0.85}As$ and AlAs layer materials and were designed using standard methods[6] and/or by considering the filter as a one-dimensional photonic band-gap structure. Our single cavity design has two Bragg mirrors, each consisting of 10 quarter-wave $Al_{0.15}Ga_{0.85}As$ / AlAs Bragg pairs, spaced by a half-wave cavity layer. Our MC-FP filter design can be visualized as in figure 6, where numbers denote a Bragg reflector containing that number of Bragg pairs, and shaded regions show the thickness (in units of the optical center wavelength λ) of higher index $Al_{0.15}Ga_{0.85}As$ cavity layers inserted between the Bragg reflectors. Fractional Bragg pair values indicate lower index AlAs spacer layers inserted between the Fabry-Perot cavities in MC-FP designs. The filter layers are grown by metal-organic chemical vapor deposition on a GaAs substrate at 710 ^oC and 80 mbar. In addition to the actual filter layer structure described above, we also inserted 10 nm thick GaAs cap layers on both sides of the filter to minimize oxidation, and a 400 nm InGaP etch-stop layer between the GaAs cap and the substrate to facilitate substrate removal.

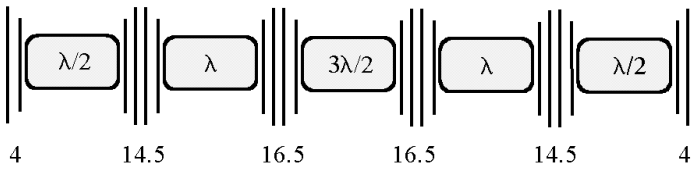

Figure 6 Layer structure of the five cavity MC-FP filter. Shaded regions represent cavities of the indicated length (in terms of the center wavelenght λ). The number of Bragg pairs in each reflector are also indicated. Fractional Bragg pairs indicate extra low-index spacer layers.

4.3 Module Assembly

Filter modules are assembled from MT ferrule tips containing 62.5 μm diameter core, graded index optical fibers. For the 2-port devices, ferrule endfacets are angled and polished at 10º to improve return loss outside the filter passband. Filter material is then attached to one ferrule with transparent epoxy. To minimize diffractive and absorptive loss in these devices, the GaAs substrate material is removed using a selective wet etch consisting of H_2SO_4:H_2O_2:H_2O, followed by selective removal of the InGaP etch-stop layer using H_3PO_4:HCl. Following these etches, the final assembly step is epoxy attachment of a second MT ferrule tip to the first, using guide pins to passively align all 12 fibers in the module simultaneously. For the 3-port modules, two ferrules are prepared at 30º and the third at 60º. Furthermore, in the three port modules, once ports 1 and 2 are assembled the filter to fiber interface is exposed through a wafer saw cut. This allows introduction of the third port. During assembly, care is required in controlling the depth of the wafer saw cut and in the longitudinal positioning of the third port. Cut depth is monitored through microscope inspection while longitudinal alignment of the third port is currently done by active alignment. A photograph of two fully assembled 3-port filter modules is given in figure 7.

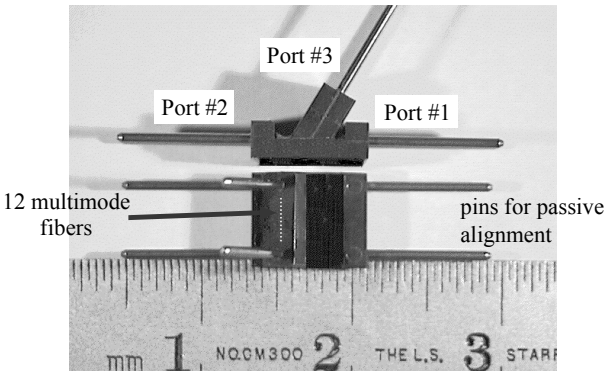

Figure 7 Photograph of 3-port filter module

4.4 Filter Module Performance

The resulting modules exhibit fiber-to-fiber separations of approximately 40 μm. Figure 8 shows the transmission characteristics for the straight-through light path (port #2) of a typical 3-port device and figure 9 shows the transmission characteristics of our 2-port filter modules. These devices exhibit low fiber-to-fiber insertion loss. For the 3-port devices the insertion losses are 1.1 dB for the port 1-2 path and 1.3 dB for the port 1-3 path. It is critical that the port 1-2 insertion loss of 3-port devices be minimized since this will ultimately limit the number of filters which can be serially cascaded in ring networks. For the 2-port devices insertion losses are 1.6 and 2.6 dB for MC- and single cavity devices, respectively.

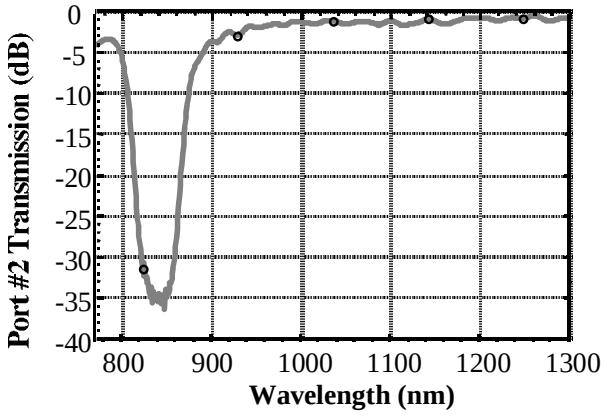

Figure 8 Transmission characteristics for port #2 of a typical 3-port filter module

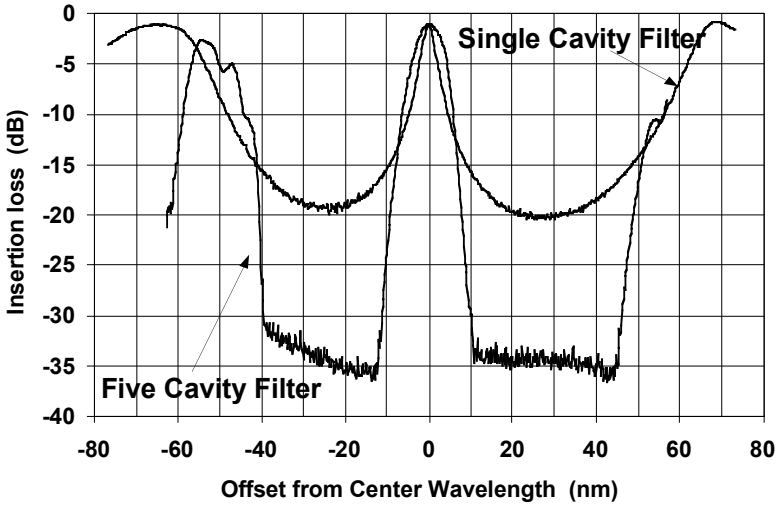

Figure 9 Transmission spectra of 2-port filter modules plotted against offset from center wavelength to highlight passband shape differences. The actual center wavelengths are 823 nm and 848 nm for the multi- and single-cavity devices respectively

The 3-port filter devices were designed to have a ~40 nm passband centered around 840 nm to be compatible with commercially available byte-wide transceivers, which are manufactured to moderate wavelength tolerances. The 2-port devices exhibit narrow passbands 7.6 nm full-width at half maximum (FWHM) for MC-FP, and 3.8 nm FWHM for single-cavity devices, respectively. Maintaining optimum filter FWHM with sharp pass-band edges is a key to achieving tightly spaced channels while allowing for transmitter drift and thermal variations. Figure 9 shows that our multi-cavity design significantly improves these features. This improvement can be quantified by the ratio of filter -3 dB bandwidth to -18 dB bandwidth, which improved from 0.13 to 0.46 for the multi-cavity design. The figure also shows improved crosstalk suppression for the multi-cavity design compared to the single cavity filter. The 35 dB suppression shown by fig. 9 is actually a lower limit set by the noise floor of our measurement system, rather than the filter characteristics. Based on this data, the MC-FP filters should provide crosstalk suppression > 23 dB for 10 nm channel spacing.

For parallel optical interconnect applications, uniform filter performance must be maintained across all the fibers within a filter module. Figure 10 shows typical uniformity results for several of our 3-port filter modules. Low insertion loss is maintained across all fibers in each module and repeatability of the assembly process is indicated by the results from more than one module. We have obtained similar uniformity results from a 2-port module, in addition to low insertion loss across all fibers, filter center wavelengths are maintained to ±0.8 nm.

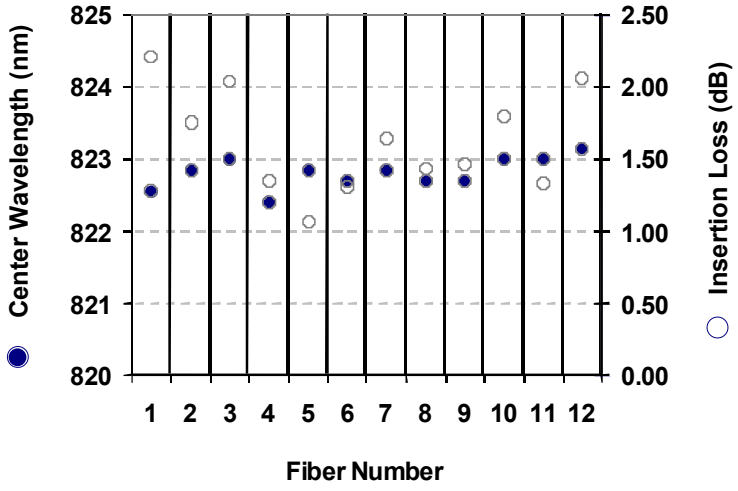

Figure 10 Uniformity data for a 2-port multi-cavity filter, center wavelength (solid markers) and insertion loss (open markers) for each fiber in the module.

4.5 Cascaded 3-Port Filter Link Demonstration

We demonstrated a dual wavelength link based on our 3-port WDM filter modules and commercially available, byte-wide transceivers (Optobahn, Optobus). 2^{23}-1 PRBS signals at ~850 and 1310nm, at bit rates of 500 and 1000 Mbit/s/fiber respectively, were routed through a cascade of up to eight filters and ~40m of 62.5µm core GRIN fiber ribbon as shown in fig. 11. This link exhibited a total insertion loss, through all 8 filters, of 10.3 dB at 1310 nm and yielded a bit error rate below $1 \cdot 10^{-14}$, including crosstalk effects between different wavelengths and different fibers in the ribbon cables. The excess power penalty for 8 filters was only 1dB. Shaking of the fiber to induce potential error rate floors had no effect, indicating that the filters introduce negligible mode selective loss.

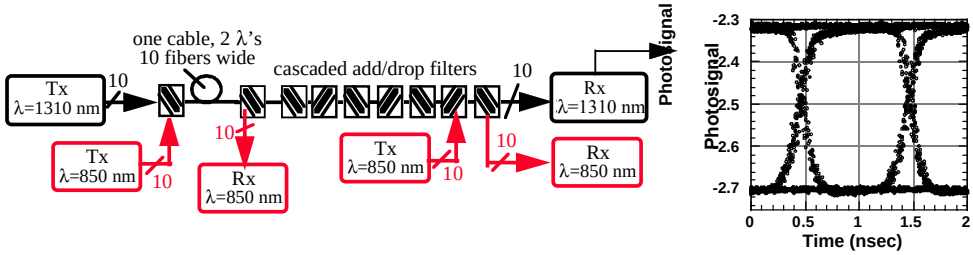

Figure 11 Schematic of 3-port filter module cascade demonstration and eye diagram for transmission through 8 filters at 1 Gb/s (λ=1310nm). Filter modules were each separated by ~4m fiber cable.

4.6 Conclusions

In conclusion, WDM filter modules for byte-wide parallel optical interconnects have been demonstrated. Filter modules suitable for add/drop multiplexing (3-port devices) and broadcast and select architectures (2-port devices) have been shown. The filter modules use low-cost plastic ferrules to provide passive alignment, and exhibit excellent transmission characteristics and channel to channel uniformity. Using multiple cavity Fabry-Perot filter designs, the 2-port devices exhibited transmission characteristics which are suitable for 10nm channel spacing. Two-wavelength byte-wide WDM operation was demonstrated using 3-port filter modules and commercial transceivers. Simulations indicate that our 3-port filter approach is suitable for 15-30 nm channel separations. These devices directly enable several interesting WDM interconnects such as chordal rings. Furthermore, when coupled with byte-wide multi-wavelength transceivers, this technology can be used to realize WDM interconnect fabrics with substantial source-routing capability and high channel bandwidth.

5. LASER SOURCES AND SYSTEM DEMONSTRATION

A necessary component for WDM links is the multiwavelength transmitter, which emits on multiple wavelength channels across multiple fibers. Single-fiber multi-wavelength sources have been demonstrated based on vertical-cavity surface emitting lasers (VCSELs)[7,8], and owing to their ease of fabrication in one- and two-dimensional arrays, VCSELs are a natural candidate for parallel fiber sources. The challenge is to multiplex in parallel a large number of wavelength channels at robust channel spacing ($\Delta\lambda$ ~ 10 nm) in a compact and efficient fashion. Here we employ a combination of direct fiber coupling and broad-band add/drop filtering to demonstrate a 4-wavelength by 10-fiber VCSEL-based transmitter in a PGA package with MT-connectorized optical output.

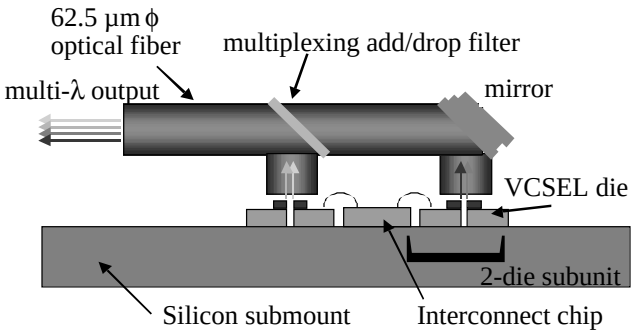

Figure 12 Cross-sectional schematic diagram of the four-wavelength transmitter. This structure is repeated on a 250 µm pitch for each of the ten fibers comprising the fiber ribbon.

A schematic diagram of the 4-wavelength parallel fiber transmitter is shown in figure 12. It consists of four single-wavelength VCSEL arrays, emitting near 825, 845, 977, or 988 nm, fastened to a silicon optical bench submount. VCSEL chips are cleaved such that the ~8 μm diameter emitter active area is centered within 15 μm of the chip edge, so that two arrays can be placed back-to-back to directly couple to the 62.5 μm core diameters of the fiber ribbon. Dual-wavelength optical signals are separately collected in bands near either 830 nm or 980 nm. These two bands are then multiplexed using a T-shaped fiber-guided add/drop filter, which is a parallel-fiber three-port device consisting of an AlGaAs/AlAs Bragg mirror embedded at 45 degrees within a fiber ribbon rigidly encased in an MT ferule. Vertical emission at the 830 nm band is reflected horizontally by the Bragg mirror and combined with 980 nm band light transmitted through the filter in the horizontal direction. A (nonmultiplexing) gold turning mirror, packaged in a similar fashion to the Bragg mirror, directs the vertical 980 nm band emission to the horizontal input of the add/drop filter. Together these turning and multiplexing optics form a fiber-guided superstrate with the four-wavelength output terminated in a MT connector. The superstrate is mated to the silicon submount using guide-pins and etched guidepin holes beneath which a second set of MT ferules are epoxied for mechanical stability. Finally, an electrical interconnect chip is placed on the submount to aid in wire bonding to the VCSEL electrical contacts, and the assembly is packaged within a standard 120 pin ceramic pin grid array (PGA).

Spectra for each of the ten output fibers of the fiber ribbon are plotted on a logarithmic scale in figure 13. VCSELs at all four wavelengths were simultaneously biased at 3 mA, and light from the ribbon cable was directed through a break-out connector and collected by an optical spectrum analyzer. Due to wire bonding difficulties, not all wavelengths were demonstrated for all fibers. Figure 14 shows the output power vs. injection current for the four emitters comprising channel (fiber) #7, showing both the total power emitted into free space without the multiplexing superstrate present as well as the multiplexed fiber-coupled output power. Coupled output power as high as –2 dBm is achieved; the lower than expected power for the 977 nm emitter is likely due to misalignment. Finally, an eye diagram showing digital modulation at 1.25 Gbit/s under a 2^{23}–1 pseudorandom bit stream (channel #3, 988 nm) is plotted in figure 15; error rates of $<10^{-14}$ were achieved. Further characterization is underway, including crosstalk between fiber channels as well as between wavelength channels within a fiber.

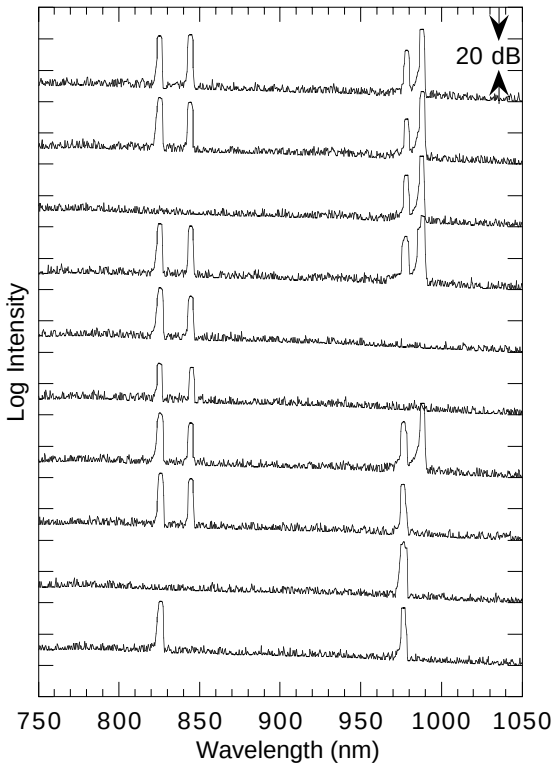

Figure 13 Output spectra for each fiber with VCSELs simultaneously biased at 3 mA each

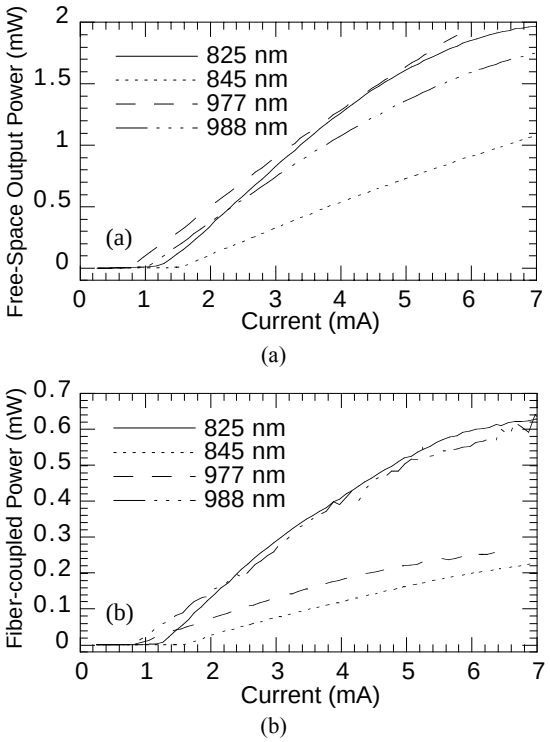

Figure 14 Light vs. current characteristics for channel #7: (a) output power into free space before fiber coupling; (b) multiplexed fiber-coupled output power

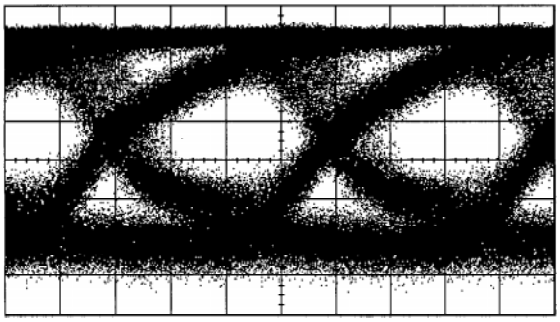

Figure 15 Eye diagram at 1.25 Gbit/s of fiber channel #3, 988 nm. The vertical axis is signal level and the horizontal scale is 200 psec/div

In summary, this is the first demonstration to our knowledge of a multiwavelength VCSEL-based parallel optical fiber transmitter. Such a device is useful for future high-bandwidth low-cost data communications applications. The use of a hybrid packaging scheme employing a fiber-ribbon-guided add/drop filter enables ten fibers by four wavelengths with a wide (>10 nm) channel spacing; more wavelengths should be achievable either by using additional filters and/or by combining this approach with monolithic techniques of achieving multiple wavelengths per VCSEL die.

ACKNOWLEDGMENTS

We thank Phil Stephan, Ted Strand, John Kerns, Stan Ault and Bill Goward of Lawrence Livermore National Laboratory for technical assistance, and Cedric Lam and Eli Yablonovitch of UCLA for a preprint of their work. This work was performed under the auspices of the U. S. Department of Energy by Lawrence Livermore National Laboratory under contract No. W-7405-Eng-48.

REFERENCES

1. Stan Ault & Mark Lowry, “A Machine-Vision Based Approach to the Problem of Low-Cost Optoelectronic Packaging,” *Proc. Surface Mount International Conference, Vol.1*, 1996, pp.383-388.
2. S. Enochs, "A packaging technique to achieve stable single-mode fiber to laser alignment," *SPIE Integration and Packaging of Optoelectronic Devices*, *Vol. 703*, p 42 (1986).
3. A recent patent describes a similar device - Blonder & MacDonald, “Article that comprises a laser coupled to an optical fiber,” *U.S. Patent #5,307,434*
4. DeGroot, A. J., Deri, R. J., Haig, R. E., Patterson, F. G., and Dijaili, S. P., “High Performance Parallel Processors Based on Star-Coupled WDM Optical Interconnects,” *Proc. 3rd Massively Parallel Processing using Optical Interconnects*, 1996, pp. 62–69.
5. Deri, R. J., et al., “Simple Fabrication of WDM Filters for Byte-Wide Multimode Cable Interconnects,” *Proc. 1998 Integrated Photonics Research.,* p. 419 (1998).
6. MacLeod, H.A., *Thin-film Optical filters*, McGraw-Hill, Colorado Springs, 1989.
7. S.-Y. Hu, J. Ko, E. Hegblom, L.A. Coldren, *IEEE J. Quantum Electron.* ***34***, pp. 1403-1414 (1998).
8. L.B. Aronson, B.E. Lemoff, L.A. Buckman, D.W. Dolfi, *IEEE Photon. Technol. Lett.* ***10***, pp. 1489-91 (1998).